

RF Lens-Embedded Massive MIMO Systems: Fabrication Issues and Codebook Design

Taehoon Kwon, *Student Member, IEEE*, Yeon-Geun Lim, *Student Member, IEEE*,
Byung-Wook Min, *Member, IEEE*, and Chan-Byoung Chae, *Senior Member, IEEE*

Abstract—In this paper, we propose a radio frequency (RF) lens-embedded massive multiple-input multiple-output (MIMO) system and evaluate the performance of limited feedback by utilizing a technique for generating a suitable codebook for the system. We fabricate an RF lens that operates at a 77 GHz (mmWave) band. Experimental results show a proper value of amplitude gain and an appropriate focusing property. In addition, using a simple numerical method—beam propagation method (BPM)—we estimate the power profile of the RF lens and verify its accordance with experimental results. Numerical results confirm that the proposed system shows significant performance enhancement over a conventional massive MIMO system without an RF lens.

Index Terms—Massive MIMO, RF lens antenna, beam propagation method, limited channel feedback, multi-variance codebook quantization method.

I. INTRODUCTION

FOR decades, researchers have studied wireless multiple-input multiple-output (MIMO) systems in an effort to provide higher capacity gains and better link reliability [2]. Work on MIMO techniques was first conducted with single-user setups, later evolving into multi-user MIMO (MU-MIMO) systems [3]. To achieve the theoretical bound of the MIMO broadcast channel where multiple antennas are deployed at both transmitter and various receivers, [4], [5] proposed simple zero-forcing (ZF)-based linear algorithms. The authors in [6] proved that a simple linear beamforming technique, referred to as coordinated beamforming, could asymptotically reach the sum capacity performance of dirty paper coding (DPC).

To support the exponentially increased mobile data traffic of the present, a need has now arisen for new techniques that go beyond conventional MIMO systems; such techniques must be able to provide at least 1000 times more capacity gains than current 4G systems [7]. Among the various candidates for such a technique, massive MIMO has emerged as a promising one [8]–[11]. By using a large amount of antennas (64 or more) at the base stations (BSs), significant improvement in network capacity and energy efficiency using ZF or maximum

ratio transmission/combining (MRT/MRC) can be expected [12], [13].

While offering a high achievable rate and energy efficiency, the equipment for a very large number of antennas at the BSs creates a host of new problems. In the case of conventional MU-MIMO systems, the feedback of channel state information (CSI) has been used to construct a precoding matrix at the BS to handle the most powerful channel modes (i.e., eigenmode) [14]. These MU-MIMO systems consider orthogonal beamforming and vector quantization as limited feedback [15], [16]. Massive MIMO systems, however, with their very large antenna arrays at the BSs, struggle to provide feedback without compression. The case of today's advanced data networks with, for example, an LTE or LTE-A requires pilot overhead that is proportional to the number of antennas. Researchers have tried to alleviate this feedback overhead problem in massive MIMO systems. They have tested channel quantization methods, including random vector quantization (RVQ) [16], Grassmannian codebook [17], and its extended version in time-varying scheme [18]; these can support a large number of users. Also, a compressive sensing-based method that fulfills the channel quantization with low complexity and low feedback overhead for users has been performed in correlated massive MIMO systems [19], [20].

What amounts to a novel approach is using, in massive MIMO systems, the radio frequency (RF) lens. Lenses are basically a phase-shifting device. They convert a divergent wavefront from a point source into a plane wave and vice versa. By providing high gain, narrow beamwidth and low sidelobes in different directions, the RF lens has been fully utilized in applications such as radars and satellite communication systems [21]. Another promising antenna design that uses RF lenses with an antenna array was proposed in [1], [22]–[27]. Traditional design has consisted of an array of antennas used with variable-length transmission lines so as to create the aperture phase profile [22]–[24].

Proposed in [25] is a discrete lens array (DLA) structure-based continuous aperture phased (CAP) MIMO at the mmWave (millimeter-wave, 60–100 GHz, region). DLA behaves as a convex lens, transferring the signals towards different points of the focal surface. Moreover, DLA narrows the beamwidth, which is still preserved in the reduced RF chain operation, making it possible to reduce the power consumption and interference between the streams. In a following work [26], the authors showed that by combining the concept of beamspace MIMO communication with a hybrid analog-digital transceiver, CAP-MIMO achieves near-optimal perfor-

T. Kwon, Y.-G. Lim and C.-B. Chae are with the School of Integrated Technology, Yonsei University, Korea (E-mail: {th_kwon, yglim, cbchae}@yonsei.ac.kr). B.-W. Min is with the Department of Electrical and Electronic Engineering, Yonsei University, Korea (E-mail: bmin@yonsei.ac.kr).

This work was in part supported by the MSIP (Ministry of Science, ICT and Future Planning), Korea, under the "IT Consilience Creative Program" (IITP-2015-R0346-15-1008) supervised by the IITP (Institute for Information & Communications Technology Promotion) and ICT R&D program of MSIP/IITP [B0126-15-1017]. Part of this work was presented in [1].

mance with dramatically lower complexity. The studies in [25], [26] mainly concern line-of-sight (LOS) mmWave channels, where there is possible only a short transmission range. The authors in [27] suggested alternative antenna designs that use an electromagnetic (EM) lens in front of a large antenna array at the BS. In the uplink setup of massive MIMO cellular systems, they demonstrated performance gains and a reduction of signal-processing complexity. What they did not consider, however, was the downlink transmission scheme, permitting the feedback overhead problem of massive MIMO systems to remain. In our prior work [1], we considered an RF lens-embedded massive MIMO system at a single-cell multi-user downlink setup. We introduced the beam propagation method (BPM) to estimate the power profile of the signal. How well the measured results agreed with our BPM-based simulations, however, was not considered by the system. In addition, lens fabrication issues have been left out of prior work.

In this paper, extending the results from [1], we study an RF lens-embedded massive MIMO system at the single-cell multi-user downlink setup, proposing a codebook design capable of enhancing the performance gain. First, we analyze the RF lens-embedded massive MIMO systems and create a new channel model. Since the channel model is directly related to the signal power profile in the proposed system, theoretical values should be accurately estimated. We adopt the BPM to calculate the propagating and focusing of incident beams controlled by the RF lens. We also investigate more details of the calculating phase profile in front of and behind the lens surface. Since the BPM simulation in [1] was based on the thin lens approximation, a more realistic analysis has to be conducted, one that includes a real experimental setup. We therefore provide measurement results and demonstrate their accordance with an analysis. Using a power profile vector acquired by BPM in designing the new codebook for the k -th user enables the quantized channel to be associated with the k -th user's power profile vector. This way the channel variance of each antenna component satisfies the multi-variance nature of our new channel model. This proposed codebook in the RF lens-embedded massive MIMO systems is termed multi-variance codebook quantization (MVCQ). We also propose several sub-algorithms that can reduce the computational complexity without notably degrading performance.

The main contributions of this paper are as follows:

- We construct a channel model and propose a new channel quantization-based codebook method for RF lens-embedded massive MIMO systems at the single-cell multi-user downlink setup. Here, we present a correlation-based massive MIMO channel model at the uplink and adapt reciprocity at the downlink. The additional power factor captured by each antenna is applied in the model. A new channel quantization-based codebook method, MVCQ, is proposed to generate adaptive codebooks that can reflect multi-channel variances caused by the RF lens antennas. We also provide numerical results that show significant throughput gain for the proposed MVCQ codebook.
- To calculate the additional power factor captured by

each antenna, we provide numerical analysis based on Fourier optics and BPM. Field distribution of RF lens is calculated by using lens geometry analysis under several assumptions. BPM—a method of calculating the propagation of a beam through a medium—is widely used to study integrated-optic structures, such as thin-film waveguides and gratings [28]. We adopt this method here in a lens-embedded system. Simulation results of BPM and its accordance with measurement results are also provided.

- We also provide the fabrication process of dielectric lens and antenna array configuration. Most prior work on lens antenna arrays paid little attention to fabrication and design issues. The physical antenna design, however, can prominently affect the performance of MIMO systems. For lens design, the parabolic lenses of different materials are tested, as the contour of both sides are well informed in closed form. This study provides radiation patterns and power profile formulas by measuring, at the receiver, insertion loss (i.e., S_{21} parameters).¹

We anticipate our contributions to yield a wide range of insights for RF lens-embedded massive MIMO systems regarding the practical fabrication issues and performance analysis.

This paper is organized as follows. Section II contains a brief overview of our proposed RF lens-embedded massive MIMO system. Basic configurations and system parameters are defined. It also gives some details of the process of constructing the channel model. Section III describes the calculating process of phase function by using the ray-tracing technique. The section also introduces algorithmic details of the beam propagation method. Note that our beam propagation method is simplified by making several assumptions, since the algorithms, to operate with the mobile devices, must be computationally efficient. Section IV demonstrates the fabrication strategy based on theoretical results and presents final antenna design and the process of design are presented. In Section V, we propose a channel feedback algorithm based on our lens-embedded channel model. Numerical results are shown in Section VI. Section VII, lastly, presents our conclusions and future work.²

II. SYSTEM MODEL

A. System Overview

We consider a single-cell multiuser downlink system where a large antenna array is equipped with the RF lens at the BS. Figure 1 offers a schematic of the proposed RF lens-embedded massive MIMO system. The BS antenna can be divided into two parts—a large antenna array part and an RF lens part. For the antenna array, we first need to determine d (the separation of adjacent antennas) and M (the number of antennas at the BS). System parameters f (the focal length

¹Our results are supported by some earlier results [29], [30].

²Throughout this paper, we use upper and lower case boldface to describe matrix \mathbf{A} and vector \mathbf{a} , respectively. The transpose and the Hermitian transpose of a matrix is notated as $(\cdot)^T$ and $(\cdot)^*$, respectively. Other notations are explained where they are used.

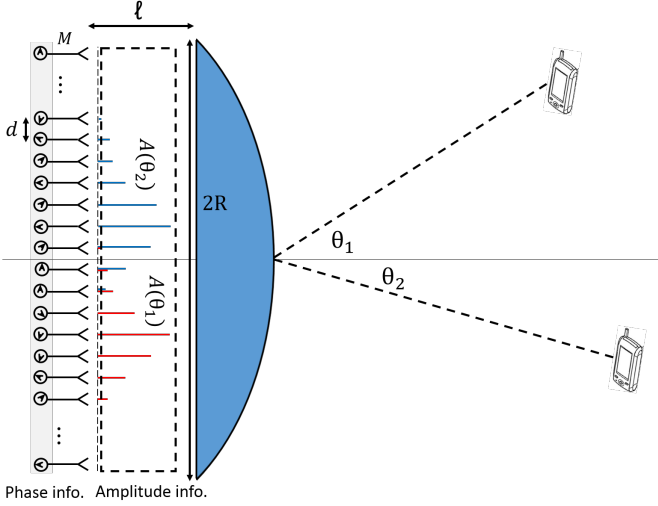


Figure 1: A schematic of the proposed RF lens-embedded massive MIMO system.

of the lens), D (the aperture diameter of the RF lens) and ϵ (the electric permittivity of lens material) should also be determined for RF lens part. The parameter ℓ (the distance between the lens and the antenna arrays) is also important, as it can determine the focusing level of the RF lens.

For array configurations, 1-dimensional (1D) uniform linear array (ULA), 2D uniform square array (USA) and circular array or even 3D antenna array configurations can be evaluated. In this paper, for simplicity, we only consider the 1D ULA.³

B. Channel Model

We first consider the channel without an RF lens. As noted above, we will restrict our attention to MIMO channels with an ULA of M antennas at the BS and one antenna at each user. Here, we adopt the spatially correlated MIMO channel model. Two popular approaches include parametric models (PMs) and nonparametric models (NPMs), which are widely used to simulate the correlated MIMO channels [31]. By choosing a suitable correlation matrix at the transmitter side, we adopt the Kronecker model, which is NPMs, to describe each channel vector between the BS and the k -th user [32]. Let θ_k be the angle where the k -th user is located. We assume a Laplacian distribution of the angle of arrival (AoA), which was widely used for the power angular spectrum (PAS), and also used in current channel models [33]. The PAS can be expressed as the truncated Laplacian pdf (probability density function), given by

$$P_\theta(\theta) = \begin{cases} \frac{\beta}{\sqrt{2}\sigma_\theta} e^{-|\frac{\sqrt{2}\theta}{\sigma_\theta}|} & : \theta \in [-\pi, \pi] \\ 0 & : \text{otherwise} \end{cases}$$

where θ is a random variable describing the offset of the mean angle for the k -th user, θ_k , σ_θ is the standard deviation of the PAS, and β is the normalization factor. In the NPMs, the coefficients of a spatial correlation matrix at the BS, given as an $M \times M$ matrix $\mathbf{R}_{k,\text{TX}}$, are described by a certain angle spread and AoA of the k -th user. Closed-form

³Future work will consider higher dimensional antenna array configurations.

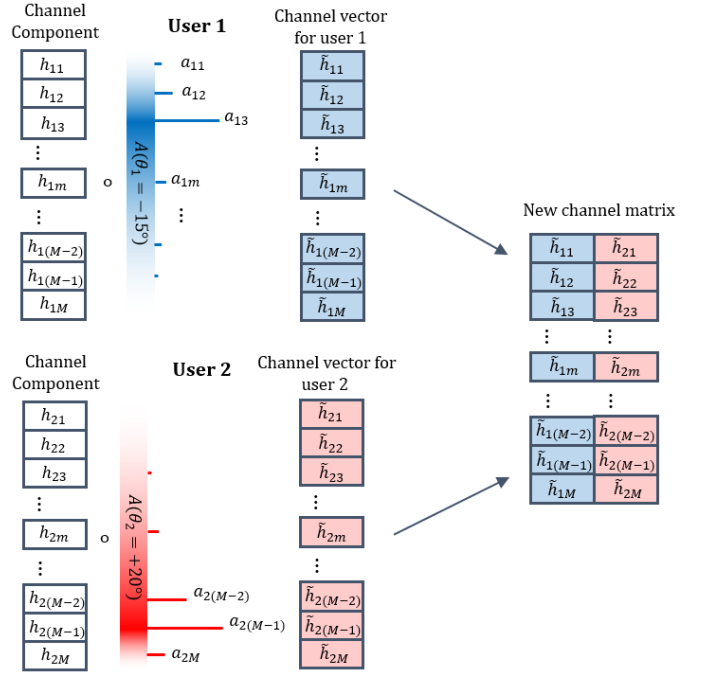


Figure 2: An example of the power distribution vectors and channel vectors for two different AoAs θ_1, θ_2 .

expression for the correlation coefficients between the i -th and the j -th antennas is derived for the Laplacian azimuth angle distribution [32].

$$[\mathbf{R}_{k,\text{TX}}(\theta_k, \sigma_\theta)]_{i,j} = \frac{\beta e^{j\kappa d(i-j) \sin \theta_k}}{1 + \frac{\sigma_\theta^2}{2} [\kappa d(i-j) \cos \theta_k]^2} \quad (k = 1, 2, \dots, K)$$

Therefore, the spatially-correlated MIMO channel between the BS and the k -th user, which is an $M \times 1$ column vector, is given by

$$\mathbf{h}_k = \mathbf{R}_{k,\text{TX}}^{\frac{1}{2}} \mathbf{h}_{\text{iid},k}, \quad (k = 1, 2, \dots, K)$$

where, $\mathbf{h}_{\text{iid},k}$ is an $M \times 1$ column vector whose elements follow the independent and identically distributed (i.i.d.) complex zero-mean, unit variance Gaussian random distribution.

Next, we consider the channel model for the proposed system in which the RF lens is deployed with the antenna array at the BS (described in Fig. 2.) Here, the presence of an RF lens enables the signal energy to be focused on a certain region of the antenna array at the BS depending on each user's AoA. We assume that the angle of arrival of the signal is equivalent to the value of the angle location of the k -th user.

Since the location of the energy-compacted region at the ULA is dependant on AoA, we define the normalized power profile vector as

$$\mathbf{a}(\theta_k) = [a_{k1}, a_{k2}, \dots, a_{kM}]^T.$$

The element a_{km} denotes the additional power factor captured by the m -th antenna at the BS. The additional power factor captured by the m -th antenna can be modeled as an integral calculus of the continuous power density function $A(\theta)$ [27]. We also define a power profile matrix $\mathbf{A} =$

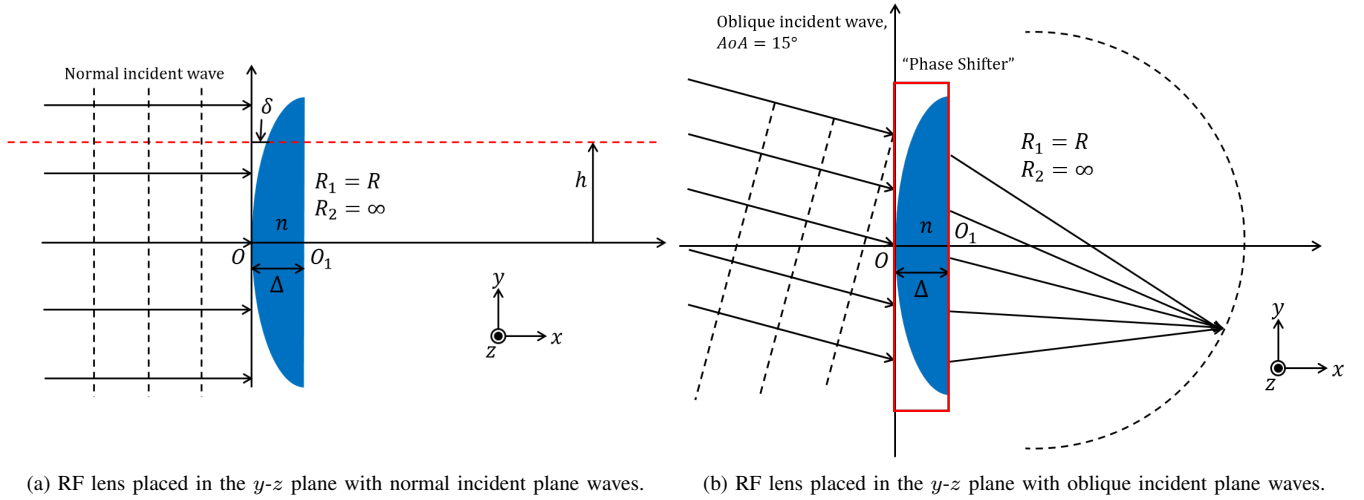


Figure 3: Wave propagation diagrams of (a) normal and (b) oblique incident waves due to RF lens placed in the y - z plane.

$[\mathbf{a}(\theta_1) \ \mathbf{a}(\theta_2) \cdots \mathbf{a}(\theta_K)]^T$ of size $K \times M$, where the rows of the matrix are the power profile vectors from all users.

Since the RF lens is a passive device with linear and invertible transfer function, we can therefore simply multiply the additional power profile vector for the k -th user to the channel vector \mathbf{h}_k without the RF lens. By adding the power profile vector, the previous channel model for the k -th user is modified to

$$\tilde{\mathbf{h}}_k = \sqrt{\mathbf{a}(\theta_k)} \circ \mathbf{h}_k,$$

where \circ is an entry-wise product of two vectors (or matrices). The modified channel matrix $\tilde{\mathbf{H}}$ for all users derived from (1) is expressed as

$$\tilde{\mathbf{H}} = [\mathbf{a}(\theta_1) | \mathbf{a}(\theta_2) \cdots | \mathbf{a}(\theta_K)]^T \circ \mathbf{H} = \mathbf{A} \circ \mathbf{H}.$$

Therefore, the received signal at the downlink transmission for the k -th user is expressed as

$$y_k = \sqrt{P_t} \tilde{\mathbf{h}}_k^T \mathbf{g}_k s_k + \sum_{j=1, j \neq k}^K \sqrt{P_t} \tilde{\mathbf{h}}_k^T \mathbf{g}_j s_j + n_k,$$

where \mathbf{g}_k , s_k and n_k denote the transmit precoding vector, the transmit symbol, and the additive white Gaussian noise vector, respectively, for the k -th user and P_t represents the total transmit power from the BS.

III. FIELD DISTRIBUTION OF RF LENS

The field distribution of the lens antenna has been studied for such applications as radar systems and communication multibeam systems. Here, we present a reversed method to analyze the plane wave signal transmitted to the RF lens with a different AoA. This kind of antenna is usually simulated using geometrical optics methods or even a tool like CST microwave studio. For computationally simple and accurate analysis, however, we conduct several analyses based on Fourier optics and BPM.

A. Phase function of the RF lens

A thin lens acts as a phase transformation, if a beam entering at coordinates (x, y) on one face emerges at approximately the same coordinates on the opposite face, that is, if there is negligible transition of the beam inside the lens. Two cases are concerned with normal incident plane waves and oblique incident plane waves as depicted in Figs. 3(a) and 3(b).

1) *Normal incident plane wave* ($\theta_{ele}, \theta_{azi} = 0$): Without an RF lens, the phase shift between $O \rightarrow O_1$ is $\Phi = \kappa \Delta$, where $\kappa = \frac{2\pi}{\lambda_0}$ illustrated in Fig. 3. With an RF lens in place, at distance h from x -axis the phase shift is given as,

$$\Phi = \kappa \left(\underbrace{\delta}_{\text{Air}} + \underbrace{n(\Delta - \delta)}_{\text{Lens}} \right) = \kappa n \Delta - \kappa(n-1)\delta$$

where δ depends on h , the ray height. Assume that lens surface is parabolic (For spherical lens, if $R \gg h$, we can take parabolic approximation as an assumption), which gives $\delta = \frac{h^2}{2R}$, so that

$$\Phi(h) = \kappa n \Delta - \frac{\kappa h^2(n-1)}{2R} \stackrel{(a)}{=} \kappa \Delta n - \frac{\kappa h^2}{2f}$$

where equality (a) is given from the lens equation,

$$\frac{1}{f} = (n-1) \left[\frac{1}{R_1} + \frac{1}{R_2} \right]_{R_1=R, R_2 \rightarrow \infty} = (n-1) \frac{1}{R}.$$

For 2D, since RF lens is placed in the y - z plane, by substituting $h^2 = y^2 + z^2$, the phase shift of RF lens is given by

$$\Phi(y, z; f) = \kappa n \Delta - \kappa \frac{y^2 + z^2}{2f}.$$

Therefore, the phase distribution $\Psi(y, z; f)$ is solely determined by the phase shift of the RF lens in the case where the normal incident plane wave is introduced.

$$\Psi(y, z; f) = \Phi(y, z; f) = \kappa n \Delta - \kappa \frac{y^2 + z^2}{2f}.$$

2) *Oblique incident plane wave* ($\theta_{ele}\theta_{azi} \neq 0$): A phase difference occurs as the ray deviates from the ray that is headed to the point of origin. We assume here that the phase shift by the lens is the same as those of normal incident plane waves, an assumption that may be inaccurate. To calculate the exact value of the phase shift function of the lens, the ray-tracing method should be considered. Here, we assume the thin lens case, so that the ray from $(0, y, z)$ at the input plane corresponds to (Δ, y, z) at the output plane. This contributes to the total phase shift at the output plane, which is represented by:

$$\Psi(y, z; f) = -\kappa\sqrt{(x \sin \theta_{ele})^2 + (y \sin \theta_{azi})^2} + \left(\kappa n \Delta - \kappa \frac{y^2 + z^2}{2f} \right).$$

B. Beam Propagation Method

Here, we introduce the numerical method that can iteratively calculate the sampled field distribution for every sampling distance Δz . We calculate the additional power factor captured by each antenna component with this method. In [34], the array response for the lens antenna array at the focal arc with critical antenna spacing is derived to be the sinc function that corresponds to the AoA of the signal. From a lens design perspective, however, not only is it hard to fabricate the negligible thickness planar dielectric lens but it is also hard to match the phase profile calculated. Also, even if it is well designed, the beams are not exactly focused in the focal arc making it hard to match the theoretical beam pattern, potentially giving rise to a discrepancy within the measured data. The BPM, which is based on traditional Fourier optics and Huygens' principle, may calculate all signal power data at any distance and at any coordinates. Also, BPM is intended to be computationally light, which may be efficient in mobile devices that actually have to estimate the channel coefficient. To simplify the mathematical analysis and reduce the computational complexity, we make several assumptions as follows:

- **RF Lens:** We assume a thin lens to simplify the analysis of phase distribution at the lens. The surface geometry is assumed to be rotationally symmetric, and the parabolic approximation is used on the lens geometry.
- **Conservation of the power:** The phase function of the lens is utilized in calculating the initial field distribution \mathbf{u}_0 at the lens surface, since the lens is a phase shifter from an EM point of view. By calculating the field distribution at the distance ℓ , we are able to acquire the fraction of the power captured by each antenna element at the BS. Due to the conservation of power, the sum of all the entries in each power profile vector is always the same.
- **Reciprocity:** BPM is used to calculate the field distribution (or power distribution) of propagating and focusing beams at the uplink transmission. Here, we assume that the BS can support users in the downlink transmission by using the same amplitude and phase profiles acquired from the uplink transmission. The amplitude and phase information of the signal at the uplink transmission can be distinctively acquired since the spatial power distribution

of an incident wave passing through the RF lens is dependent on the AoA. We can, therefore, use these values as profiles for the downlink.

1) *Scalar representation of wave equation:* Since the vector wave equation is obeyed by both E -field and H -field, an identical scalar wave equation is obeyed by all components of those vectors. Thus, for example, x component of E -field obeys the equation

$$\nabla^2 E_x - \frac{n^2}{c^2} \frac{\partial^2 E_x}{\partial t^2} = 0$$

and similarly for E_y, E_z, H_x, H_y , and H_z . Therefore, it is possible to summarize the behavior of all components of \vec{E} and \vec{H} through a single scalar wave equation,

$$\nabla^2 u(s, t) - \frac{n^2}{c^2} \frac{\partial^2 u(s, t)}{\partial t^2} = 0$$

where $u(s, t)$ represents any of the scalar field components (s : position, t : time). The scalar field may be written explicitly as $u(s, t) = \text{Re}\{U(s) \exp(-j2\pi vt)\}$, where $\text{Re}\{\cdot\}$ signifies "real part of", and $U(s)$ is a complex function of position. We use the concept of instantaneous intensity defined as $I(s, t) = |U(s)|^2 = |u(s, t)|^2$.

2) *Beam propagation method:* From Fourier optics, the propagations of EM waves through the RF lens can be expressed as follows [35]:

$$U(x, y) = \frac{e^{jkz}}{j\lambda z} \mathcal{F}^{-1} \left[\mathcal{F}\{U(x', y')\} \circ \mathcal{F}\left\{e^{j\frac{k(x'^2 + y'^2)}{2z}}\right\} \right],$$

where \mathcal{F} denotes the Fourier transform operator, $U(x', y')$ is the field distribution at the aperture, $U(x, y)$ is the field diffraction pattern at distance z , and $e^{jk(x'^2 + y'^2)/(2z)}$ is the quadratic phase factor. When this approximation is valid, the observer is said to be in the near field of the aperture. The surface geometry is assumed to be rotationally symmetric, and the focal points are placed on its axis. When the beam has a certain angle of arrival (AoA), off-axis aberrations are ignored.

BPM is used to calculate the field distribution (or power distribution) of propagating and focusing beams at the uplink transmission. The phase function of the lens is utilized in calculating the initial field distribution \mathbf{u}_0 at the lens surface, since the lens, from an EM point of view, is a phase shifter. By calculating the field distribution at the distance ℓ , we are able to acquire the fraction of the power captured by each antenna element at the BS. According to the conservation of power, the sum of all the entries in each power profile vector is always the same. Introduced here is a numerical method that calculates the power profile vector of the RF lens. If the initial field distribution at the lens surface is given as \mathbf{u}_0 , we can inductively calculate the next step of field distribution; the Fourier transform of the current field distribution is multiplied by the wave system function \mathbf{h}_{sys} [28].

$$\begin{aligned} \mathbf{u}_n &= \frac{e^{jk\Delta z}}{j\lambda\Delta z} \mathcal{F}^{-1} [\mathcal{F}\{\mathbf{u}_{n-1}\} \circ \mathbf{h}_{\text{sys}}], \\ \mathbf{h}_{\text{sys}} &= \mathcal{F}\left\{e^{j\frac{k(m\Delta x)^2}{2\Delta z}}\right\}, \end{aligned} \quad (1)$$

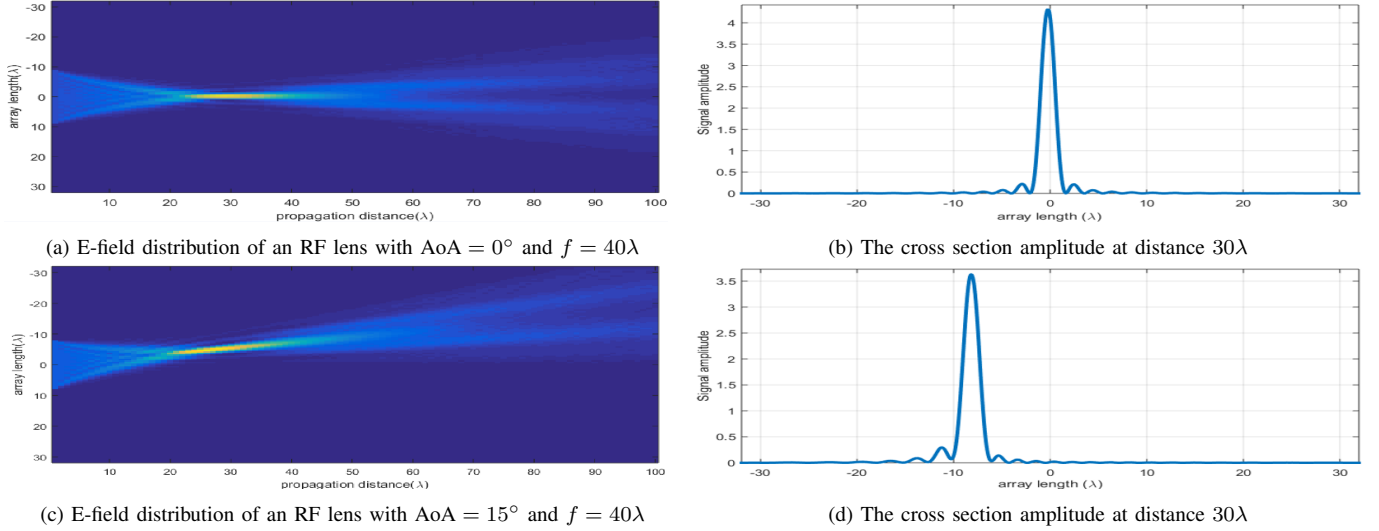


Figure 4: Propagating and focusing property of incident wave to the lens.

G. Focal Length	20λ	30λ	40λ	50λ
Peak Distance	16λ	20λ	27λ	33λ
Focusing Intensity	6.11x	4.92x	3.47x	2.88x

Table I: Beam propagation of focused beams with geometrical focal lengths of 20λ, 30λ, 40λ, and 50λ.

where Δx and Δz denote the sampling distance on the x - and z -axes. \mathbf{u}_n is the E-field distribution at distance $d = n\Delta z$ from the RF lens.

Figure 4 illustrates, using the BPM algorithm, the propagating and focusing properties of a wave through the RF lens. For the RF lens with 20λ, 30λ, 40λ and 50λ of geometrical focal length, the beam width, peak distance, and field intensity are calculated in Table I. Starting from the aperture of the lens, which is given as 20λ, an iterative propagation method is adapted where the sampling distance Δx and Δz are 1λ and 1λ, respectively. The difference between the geometric focal length and peak distance is observed, which corresponds well with diffraction theory [36]. The field intensity of the wave is intensified by 6.11, 4.92, 3.57 and 2.88 at the peak distance of the wave.⁴

IV. MEASUREMENT SYSTEM

To investigate the accordance between the measurements of the power in front of the RF lens and the BPM result, a field measurement system was constructed. Since the performance of an codebook significantly depends on the estimation of power distribution shape of the RF lens, a more accurate characterization for the power distribution function of the RF lens is desirable. The measurements were carried out at 77 GHz; the following discussions and all the results refer to

⁴In practice, the radiated beam from a horn antenna is calculated accurately with the modified multimode Gaussian beam and transferred through the lens using ray tracing. Also, the previous discussion of an RF lens and BPM considered a thin lens approximation. Since we attempt to find an accurate data, for future work, thick lens analysis will be carried out with more practical setup.

this frequency. The measurement results are compared with the results obtained by BPM. A 77 GHz patch antenna was designed and fabricated as shown in Fig. 6(a), for lens-antenna integration. Two PCB layouts were designed: a single patch antenna that was used for the probe antenna and a 65-cross-aligned patch antenna array. The latter was deployed as an actual BS antenna design. Details of system components are explained below.

A. RF Lens

The design principles of lenses are very well known. Geometric optics was the one and the only thing that needed to be considered when ignoring secondary effects like edge diffraction, surface, or radiating element impedance mismatch. Here, we consider lens curvature as one of the simplest cases, hyperbolic lens with dielectric material.

The dielectric constant of the lens is ϵ_r , which is the square of the refractive index, n . Conditions imposed on a dielectric lens is the electrical path length constraint and Snell's law [37]. The contours of a few classical lenses (including the hyperbolic lens) can be described by simple analytic formulas. In the simplest case, which is a hyperbolic lens with a flat surface on S_2 , the contour of S_1 is given by

$$y_1 = [(n^2 - 1)(x_1 - f)^2 + 2(n - 1)(x_1 - f)f]^{\frac{1}{2}}.$$

This can be reformulated as below.

$$y_1^2 = \underbrace{(n^2 - 1)}_A \left(x_1 - \underbrace{\frac{n}{n+1}f}_B \right)^2 - \underbrace{\frac{n-1}{n+1}f^2}_C.$$

If the values of focal length and the diameter of the lens are fixed, a certain value of thickness must be used to fulfill the focusing property of the lens, which is given by

$$T = \frac{1}{n+1} \left\{ \left[f^2 + \frac{(n+1)D^2}{4(n-1)} \right]^{\frac{1}{2}} - f \right\}.$$

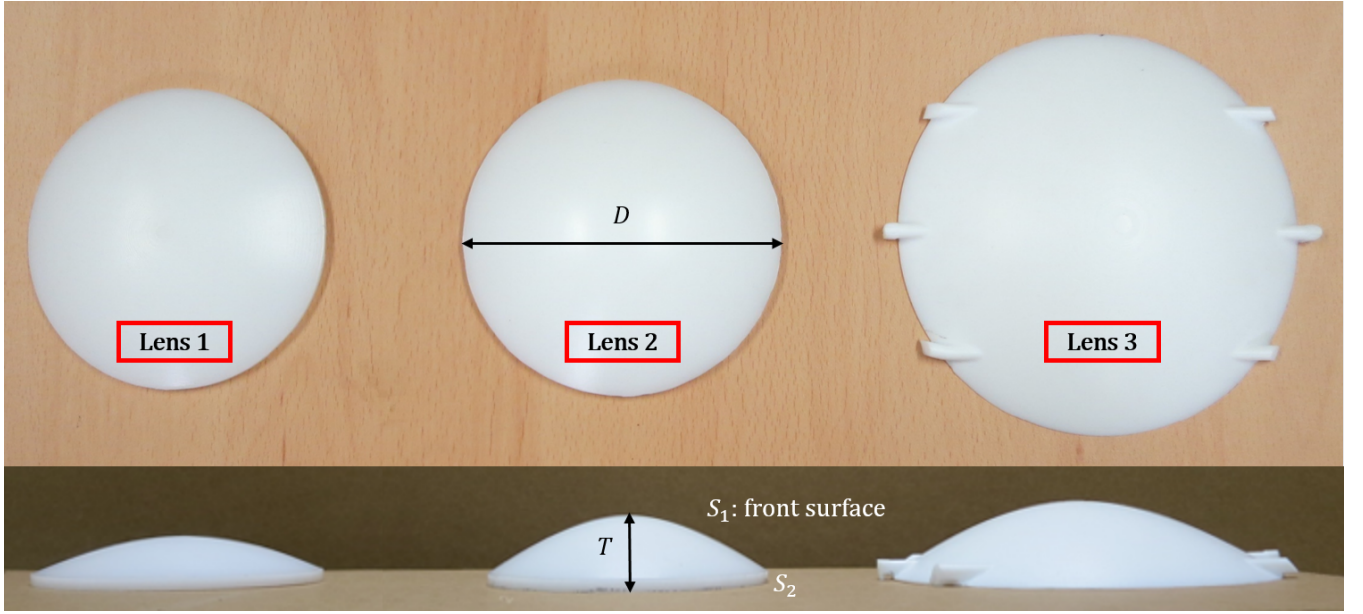


Figure 5: Fabricated dielectric lenses.

Lens Index	Material	ϵ_r	f (mm)	D (mm)	f/D	T (mm)	Contour (A, B, C)
1	Polyethylene	2.40	140.3	116.8	1.2	18.9	(1.4, 85.24, 4238.30)
2	Polyethylene	2.40	93.5	116.8	0.8	24.8	(1.4, 56.83, 1883.70)
3	Teflon	2.06	162	135	1.2	26.9	(1.06, 95.48, 4690.68)

Table II: Geometry of fabricated dielectric lenses.

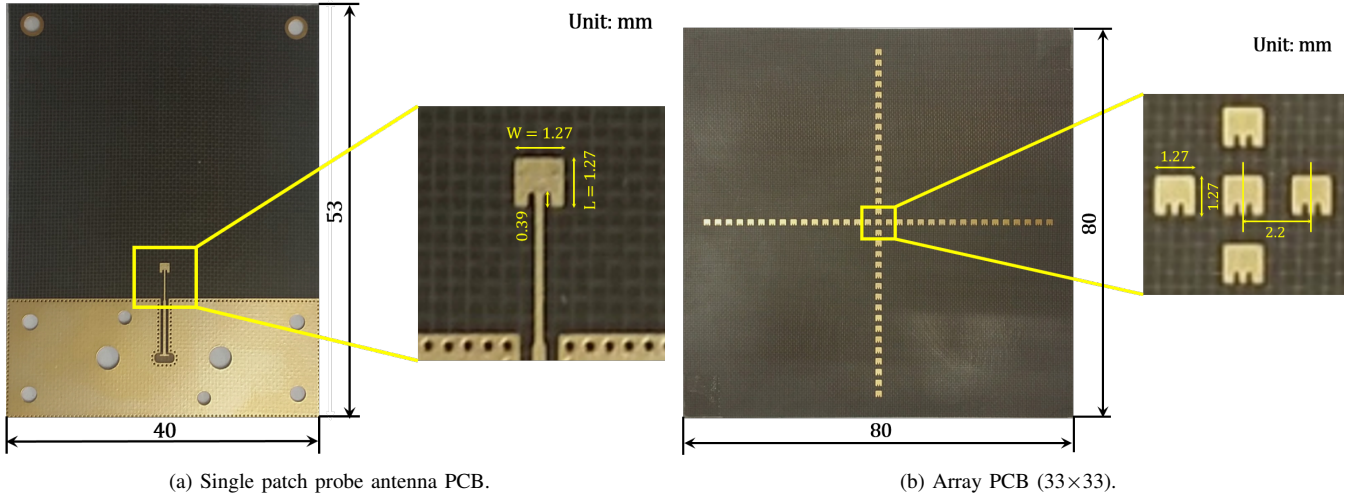


Figure 6: Configuration of a single patch antenna and array layout.

Based on this theoretical background, several dielectric lens designs were considered. For lens material the study used Teflon ($\epsilon_r = 2.06$) and Polyethylene ($\epsilon_r = 2.40$). The focal length, aperture, thickness, f/D ratio and curvature parameters A, B, C were calculated according to Table II.

B. Experimental Setup

1) *Transmitter*: Used at the transmitter was a horn antenna operating at 70–80 GHz. The power from an oscillator, tunable from 70–80 GHz, was fed through a 0–50 dB calibrated

attenuator to the transmitting horn. Reflector was used to lengthen the distance between the transmitter and receiver.

2) *Receiver*: What is desirable, for proper antenna design, is small size, low directivity, and fairly equal E – and H –plane amplitude patterns. The antenna component was fabricated on 0.127 mm thick Taconic TLY-5 substrate ($\epsilon_r = 2.18$, loss tangent = 0.0075). For the array design, the dimensions were $W = 1.27$ mm, $L = 1.27$ mm. The fabricated patch antennas were aligned in a cross-section where 65 patch antennas (33×33) were used. Array spacing between patches was given as 2.2 mm, which is 0.56λ at 77 GHz. During

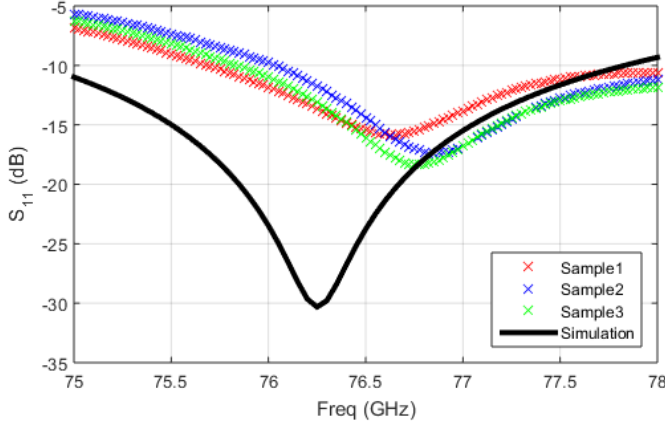


Figure 7: Simulation and measured S_{11} parameter data of a single patch probe antenna.

all the measurements, an absorber was placed at the back of antenna and the lens antenna. In the measurements, a single patch probe antenna was attached at the antenna mounting part. A styrofoam jig, with absorbers attached to the surface, was designed to fix the location of the fabricated RF lens. The center of the lens was aligned with the transmitter and the receiver.

C. Measurement procedure

The measurement was held in an anechoic chamber. To calibrate the measurement system, a horn antenna was used with standard gain at 77 GHz. To decide the spatial power profiles of the propagating beams toward the lens, the probe antenna should be placed at different positions along x (H -plane) and y (E -plane). Considering the alignment problem of the chamber, however, rather than moving the probe antenna, experimenters moved the styrofoam jig back and forth, as shown in Fig. 8. The radiation pattern of the receiver antenna was also measured by rotating the antenna in the range of $[-15^\circ, 15^\circ]$ in the azimuth and elevation angle domains. Three types of fabricated lenses in Table II were used. For each configuration, measurements were held three times by using three sample probe antennas. Presented below are the details of the procedures.

- 1) First, the measurements were conducted without an RF lens. Calibration was done initially and S_{11} parameters were measured for each antenna sample. The radiation pattern of the receiver antenna was measured for the range of $[-90^\circ, 90^\circ]$ in both the elevation and azimuth angle domain. This was conducted to see the effect of the metal jig attached to the patch antenna in the fabrication process (Fig. 6(a)). The radiation pattern of the single patch probe antenna without the RF lens was also measured to see the pure receiver antenna gain.
- 2) Installing the RF lens-attached styrofoam jig in front of the antenna mounting part allowed us to consider the effect of the RF lens. Each component was covered with an absorbing material to minimize the external factor that may affect the field distribution pattern. The distance from the lens was changed by the 20 mm steps starting from the 40 mm. Azimuth and elevation radiation

patterns were measured for the range of $[-15^\circ, 15^\circ]$ in both the azimuth and elevation angle domains. The axial power distribution was measured on the assumed axis of the beam.

- 3) The procedures above were repeated for all three fabricated lenses and three different probe antenna samples. In total, 90 measurement configurations ($3 \times 3 \times 10$) were formulated to see the results.

D. Experimental Result

The measurements were carried out with different lenses, different probe antenna samples, and lens separations. To measure the radiation pattern, the antenna was rotated in the range of $[-15^\circ, 15^\circ]$ in both the azimuth and elevation angle domains. As the axial power distribution was measured, the separation between the lens and probe was altered, in each configuration, in 20 mm steps, resulting in an axial measurement range of 40 mm–220 mm.

Step 1), the measurement without the RF lens, was performed to demonstrate the basic properties of the designed probe antenna samples. The S_{11} parameter in the range of 75 GHz–78 GHz in Fig. 7 showed a difference between the simulation and the measurements, where the center frequencies of the designed samples were slightly higher than that of the simulation. This was the expected error caused by the fabrication process since the physical dimensions of the antenna were so small thus it could mismatch the simulation result.

The study also evaluated the elevation and azimuth radiation patterns of fabricated probe antenna samples. The agreement between elevation and azimuth radiation pattern should hold since we assumed fairly equal amplitude radiation patterns. A slight discrepancy, however, was observed between the elevation and azimuth radiation patterns at $[-90^\circ, -30^\circ]$ since the reflection from the metal jig affected the elevation radiation pattern. Nearly the same level of antenna gains was measured in the other θ region, especially $[-15^\circ, 15^\circ]$ for the measurement with lens. The 3 dB beamwidth and peak gain for the azimuth pattern were 95° and 5.73 dBi.

Step 2), the measurement with an RF lens, was designed to evaluate the beam characteristics in front of the RF lenses. Figures 9(a), 9(c), and 9(e) compare the azimuth radiation patterns of the lens and no lens cases. The distance between the lens and receiving antenna is carefully decided based on the focal length of the fabricated lens. All three lenses showed an amplitude gain exceeding 20 dB, at the azimuth angle with peak value. The lens property of focusing the power of incident wave was thus verified, even considering the loss tangent of materials [38].⁵

The axial power distributions of the beam in front of each lens are shown in Figs. 9(b), 9(d) and 9(f). The blue one is a BPM simulation result that assumes each dielectric parabolic lens to be a thin spherical lens with equivalent focal length. A parabolic lens was chosen over a thin spherical lens owing to fabrication issue; since a parabolic lens has a closed form contour for both sides while a spherical lens

⁵The beams are not exactly centered due to the misalignment of the styroform jig.

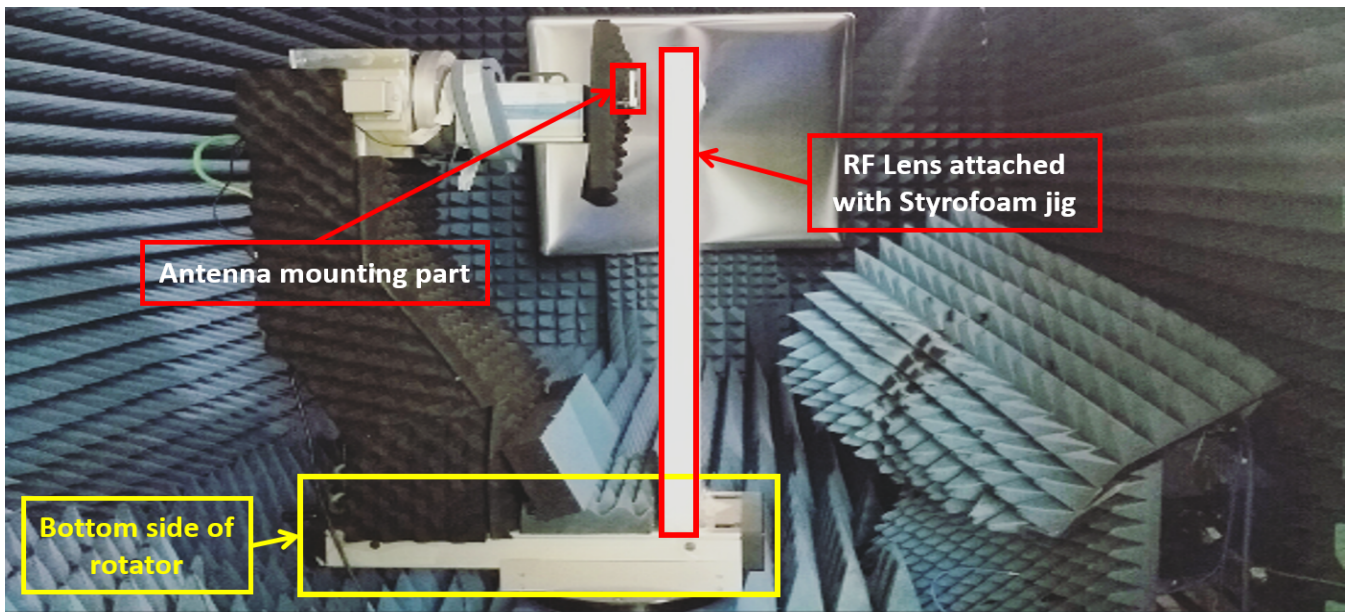
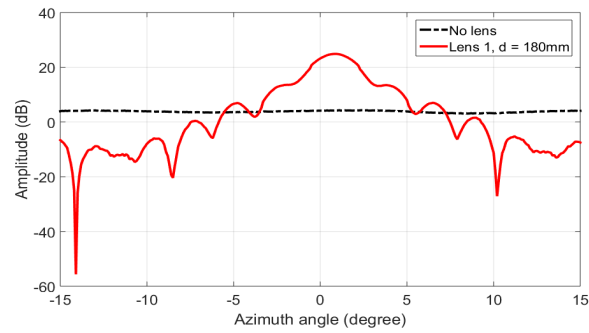
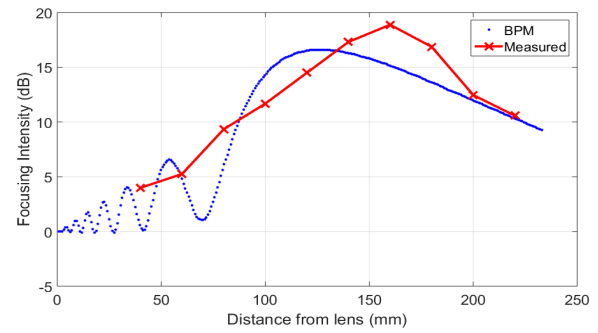


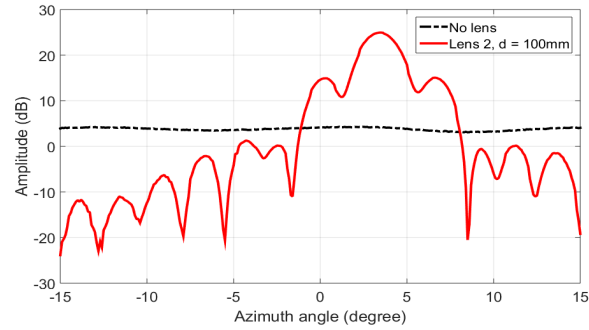
Figure 8: Characterization and measurement setup.



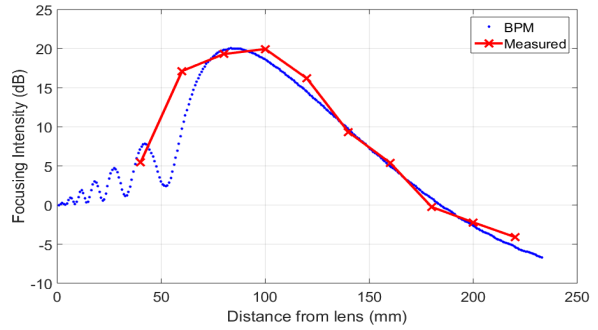
(a) Azimuth radiation pattern with Lens 1



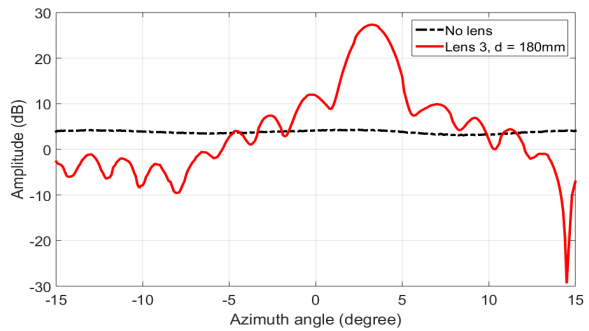
(b) Axial power distribution (focusing intensity) of Lens 1



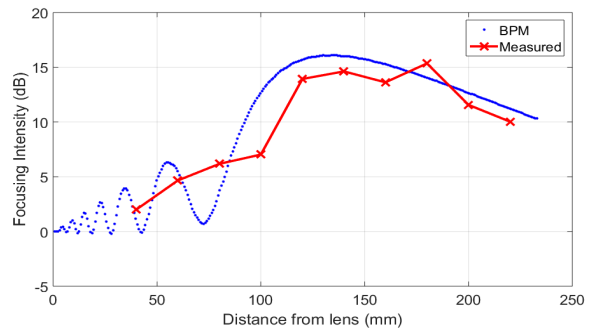
(c) Azimuth radiation pattern with Lens 2



(d) Axial power distribution (focusing intensity) of Lens 2



(e) Azimuth radiation pattern with Lens 3



(f) Axial power distribution (focusing intensity) of Lens 3

Figure 9: Azimuth radiation pattern and axial power distribution of three different lens antenna setup.

does not. We therefore only compare focusing intensity in these measurements. It is widely known that the thin lens approximation breaks down for the lens with a small f/D ratio, but focusing intensity has comparable results with the thin lens assumption.

Possible sources of error in the measurements are numerous. These include inaccuracies of the moving styrofoam jig, alignment problem of transmitter, lens, and receiver, directivity of the probe antenna and standing waves between the lens and receiver. The measurement interval at the axial measurements is 20 mm; this means that a maximum 10 mm inaccuracy could occur. Also, errors caused by misalignment of the horn, lens and probe antenna should be amended for each configuration. We leave these for our future work.

V. PROPOSED CHANNEL FEEDBACK ALGORITHM

Now we consider limited feedback methods using a channel-quantized codebook. Let $\mathbf{C} = [\mathbf{c}_1 | \mathbf{c}_2 \dots | \mathbf{c}_N]$ be a codebook with its cardinality N (a positive integer), and \mathbf{C} is known to be at both the BS and users. The beamforming vector that maximizes the inner product with the actual channel vector will be chosen from codebook \mathbf{C} . Thus, the codebook index j_k , selected for the k -th user, can be acquired from the formula: $j_k = \arg_j \max |\mathbf{h}_k^* \mathbf{c}_j|$. In practical systems, the users only need to feed back an index of the codebook vector j_k that correlates the best with their channel vector. Here we briefly introduce RVQ, which is a conventional and widely used method in MIMO systems. We, then, propose a new method to generate an adaptive codebook for our system model.⁶

A. Random Vector Quantization (RVQ)

One of the easiest and most adaptable ways to design a codebook is to generate one in random. In RVQ beamforming with the feedback bits B , a codebook is generated as $\mathbf{W} = [\mathbf{w}_1 | \mathbf{w}_2 \dots | \mathbf{w}_{2^B}]$ of size $M \times 2^B$ complex matrix. The column vector \mathbf{w}_j ($j = 1, 2, \dots, 2^B$) denotes the codebook vector. Note that the each column $\mathbf{w}_j = [w_{j1} | w_{j2} \dots | w_{jM}]^T \sim \mathcal{CN}(0, 1)$. In a spatially-correlated channel, the RVQ codebook, \mathbf{W}_{rvq} , is given as, $\mathbf{W}_{\text{rvq}} = (\mathbf{W}^T \mathbf{R}_{\text{TX}}^{\frac{1}{2}})^T = [\mathbf{w}_1 | \mathbf{w}_2 \dots | \mathbf{w}_{2^B}] \in \mathbb{C}^{M \times 2^B}$. If a codebook index is chosen as j , the estimated channel at the BS is selected as $\hat{\mathbf{h}}_k = \mathbf{w}_j$.

B. Multi-Variance Codebook Quantization (MVCQ)

Here, we propose a new feedback algorithm based on RVQ by considering the power profile vectors of the users. Under the presence of the RF lens within the ULA at the BS, the conventional RVQ cannot reflect the changed channel characteristics of different variances. Since our system model assumes that the users are forward fed the information of the angle where they are located in a cell, they can exploit the power profile vectors in their codebook designs. The channel vectors associated with the antennas at the BS have different variances since the energy is focused on a subset of antennas at

the ULA after passing through the RF lens. We can therefore simply multiply the m -th power profile element to the m -th element of the conventional RVQ codebook vector so that the variance of each entry in the constructed codebook vector will shift to the desired level. Thus, the entries of the new codebook vector for the k -th user are made to have different variances $a_m(\theta_k)$, and we call this new channel quantization method, MVCQ. Thus, the proposed codebook $\mathbf{W}_{\text{mvcq},k}$ for the k -th user is expressed as

$$\begin{aligned} \mathbf{W}_{\text{mvcq},k} &= [\sqrt{a(\theta_k)} \circ \mathbf{w}_1 | \sqrt{a(\theta_k)} \circ \mathbf{w}_2 \dots | \sqrt{a(\theta_k)} \circ \mathbf{w}_{2^B}] \\ &= [\mathbf{w}'_1 | \mathbf{w}'_2 \dots | \mathbf{w}'_{2^B}], \end{aligned}$$

where \mathbf{w}'_j , the column vector of $\mathbf{W}_{\text{mvcq},k}$ follows the distribution of, $\mathbf{w}'_j = [w'_{j1} | w'_{j2} \dots | w'_{jM}]$, $w'_{jm} \sim \mathcal{CN}(0, a_m(\theta_k))$. For the other users, the proposed codebook can be defined as the same way.

We can analyze, roughly, the effect of MVCQ in terms of the power correlation matrix and signal-to-noise-plus-interference ratio (SINR). The power correlation matrix Ψ is defined as $\Psi = \sqrt{\mathbf{A}^T} \sqrt{\mathbf{A}}$, where \mathbf{A} is the power profile matrix. The power correlation matrices for the system without the RF lens ($\Psi^{(1)}$) and with the RF lens ($\Psi^{(2)}$) are given, respectively, as,

$$\Psi^{(1)} = \begin{pmatrix} 1 & 1 & \dots & 1 \\ 1 & 1 & \dots & 1 \\ \vdots & \vdots & \ddots & \vdots \\ 1 & 1 & \dots & 1 \end{pmatrix}, \Psi^{(2)} = \begin{pmatrix} 1 & r_{1,2} & \dots & r_{1,K} \\ r_{2,1} & 1 & \dots & r_{2,K} \\ \vdots & \vdots & \ddots & \vdots \\ r_{K,1} & r_{K,2} & \dots & 1 \end{pmatrix},$$

where $r_{j,k} = r_{k,j} = \sqrt{a(\theta_j)^T} \sqrt{a(\theta_k)} / M$. Since $\mathbf{a}(\theta_k)/M$ is a normalized power profile for the k -th user, $r_{j,k} = r_{k,j} = \sqrt{a(\theta_j)^T} \sqrt{a(\theta_k)} / M < 1, \forall j \neq k$ and $r_{k,k} = 1$. Also, SINR for the k -th user is approximated as

$$\text{SINR}_k \simeq \frac{P_t / K \Psi_{k,k}^{(i)} |\mathbf{h}_k^T \mathbf{g}_k|^2}{P_t / K \sum_{j=1, j \neq k}^K \Psi_{k,j}^{(i)} |\mathbf{h}_k^T \mathbf{g}_j|^2 + 1},$$

where $i = 1$, or 2 for the system without or with the RF lens, respectively.

While all the elements in $\Psi^{(1)}$ are 1, $\Psi_{k,j}^{(i)}, k \neq j$, which denotes the off-diagonal term of $\Psi^{(2)}$, they can be decreased to less than 1. This implies that the desired signal power term is the same for both cases while the interference power term of SINR is greatly decreased in the RF lens-embedded massive MIMO systems. We can, therefore, insist that MVCQ improves the SINR for those users who are sufficiently resolvable at the BS.

C. Low Complexity Estimation Methods

The performance of an MVCQ critically depends on the estimation accuracy of power distribution, which corresponds to the additional coefficients $\mathbf{a}(\theta_k)$. It is, therefore, to have a more accurate characterization for the power distribution function of the RF. However, the computationally 'heavy' nature of an iterative algorithm may be hard to adapt to a real mobile device. We therefore introduce a power distribution function or sub-algorithms that can be simply adapted to the MVCQ. By coarsely approximating the power distribution function as a well-known distribution like a Gaussian function,

⁶The proposed codebook is available at <http://www.cbchae.org/>.

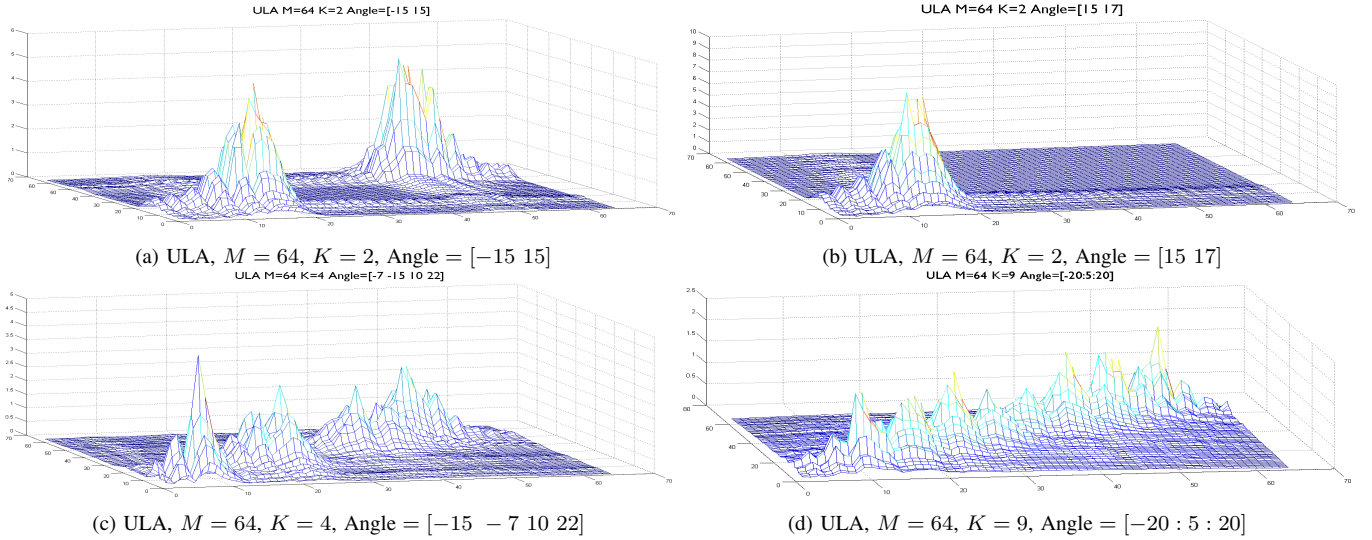


Figure 10: Unnormalized channel correlation matrices of various user scenarios.

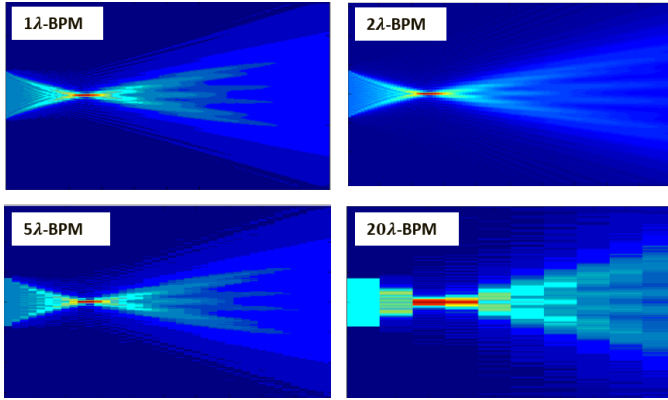


Figure 11: Sub-BPM.

the system has to decide only a few parameters to estimate the power distribution.

1) *Gaussian*: The normalized Gaussian power distribution can be adapted. To specify the function, peak power location, y_θ , and average power spread, V_θ , should be decided. The power distribution function is given as,

$$a(y; \theta) = \frac{1}{\sqrt{2\pi V_\theta}} \exp \left(-\frac{(y - y_\theta)^2}{2V_\theta} \right),$$

where y_θ and V_θ should be decided from the experimental results.

2) *Sub-BPM*: Since BPM is an iterative propagation algorithm, sampling can be done more sparsely to estimate the power distribution. From (1), the sampling distance Δz can be changed freely. Figure 11 shows the BPM simulation results of changing sampling distance by 1λ , 2λ , 5λ , and 20λ . Simulation parameters are the same as the parameters in Fig. 4(a). As the sampling distance increases, the estimation accuracy wanes while the complexity of the algorithm decreases.

VI. PERFORMANCE ANALYSIS

We consider here a single-cell downlink transmission and feedback scenario where $M = 64$ with adjacent antennas separated by $d = 0.5\lambda$ at the BS. The geometry of the RF lens

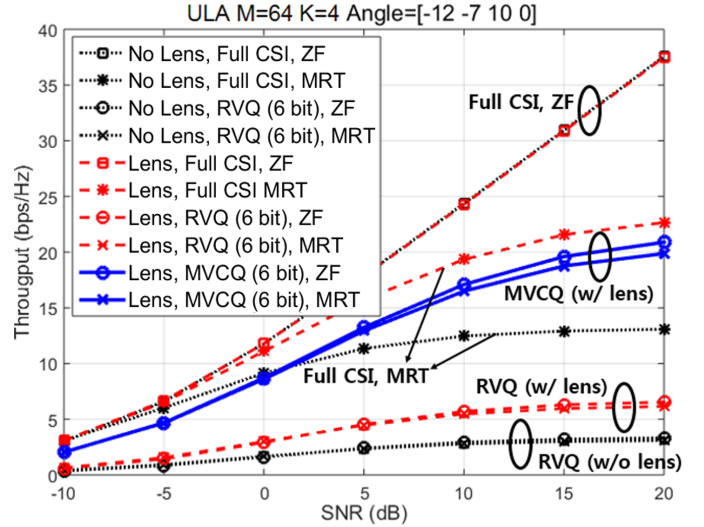


Figure 12: Achievable sum rate of massive MIMO systems with and without the RF lens.

is given as $\ell = 25\lambda$ and $f = 40\lambda$. The electric permittivity of the lens is set to be 2.4. The power profile vectors vary with the angles where users are located, so various angles are tested. The coverage angle of the antenna array is specified to the range $[-30^\circ, 30^\circ]$, for the case of six equally covered sectors in a cell. Zero forcing (ZF) and maximum ratio transmission (MRT) precoders are implemented based on the estimated channel.

Figure 10 illustrates several channel correlation matrices $\mathbb{E}[\tilde{\mathbf{H}}^* \tilde{\mathbf{H}}]$ for the various number of users and the angles. In Fig. 10a, two energy-focused peaks are resolvable, which implies that there is enough angle difference between the two users. In Fig. 10(b), however, the channels of two adjacent users are hard to separate at the BS, which means we need more antennas at the BS to distinguish one user from another. Figure 10(c) and Fig. 10(d) deal with multi-user cases (four and seven users, respectively). If a sufficient angle distance is guaranteed between the users, the performance of the RF lens-

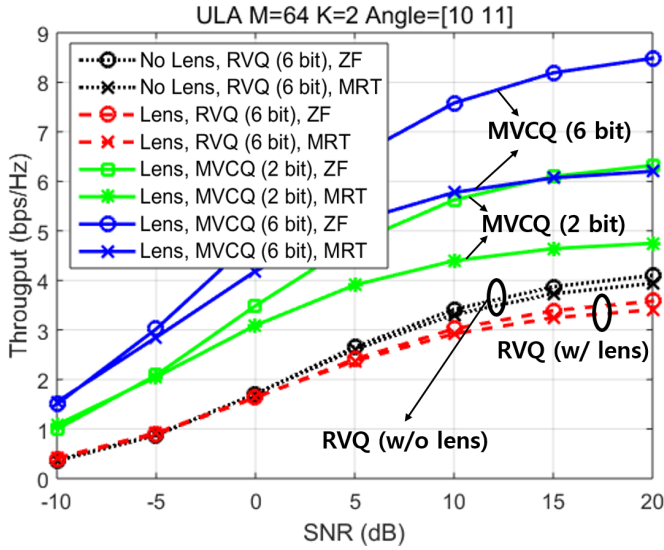


Figure 13: Achievable sum rate of massive MIMO systems with and without the RF lens (2 bit feedback included).

embedded system is not likely to be degraded significantly. From the channel correlation matrix of specific user cases, we can estimate the performance of our proposed system.

Figure 12 plots the achievable sum rate of the massive MIMO system with and without the RF lens. In total, 64 antennas are deployed at the BS with four users having -12° , -7° , 10° , and 0° in a cell. A transmitter performs knowing the full CSI or a quantized CSI that uses a limited feedback method using RVQ and MVCQ (the proposed scheme). For MVCQ codebook generation, 1λ -BPM is used. If the full CSI is known to the BS, the MRT precoder has a slight throughput gain while the ZF precoder remains unchanged. Regardless of the deployment of the RF lens, in limited feedback cases where the 6 bit RVQ codebook is used, no performance gap is found between the two systems. This means that the RVQ is not suitable for the RF lens-embedded massive MIMO systems; in fact, it may even be worse than not using an RF lens. When the MVCQ method with the 6 bit codebook is used for the channel estimation, both the ZF and MRT precoders show a steep increase in their performances. They perform nearly comparably to the MRT precoder with full CSI at the system with the RF lens. Both MVCQ scenarios outperform the MRT precoder with full CSI at the system without the RF lens at the high SNR regime. We can conclude, therefore, that, to achieve the desirable performance, the proposed system needs only a few bits.

In Fig. 13, we consider the RF lens-embedded massive MIMO system with the BS equipped with 64 antenna elements and two neighboring users located in a single cell, with an angle domain of 10° and 11° each. For MVCQ codebook generation, 1λ -BPM is used. Since the angle difference between the two users is comparatively small, it is expected that the performance of the lens-embedded massive MIMO system might be degraded due to the difficulty of resolving the signal from two different users at the BS. Also, the performance of ZF precoder is far better than that of the MRT precoder.

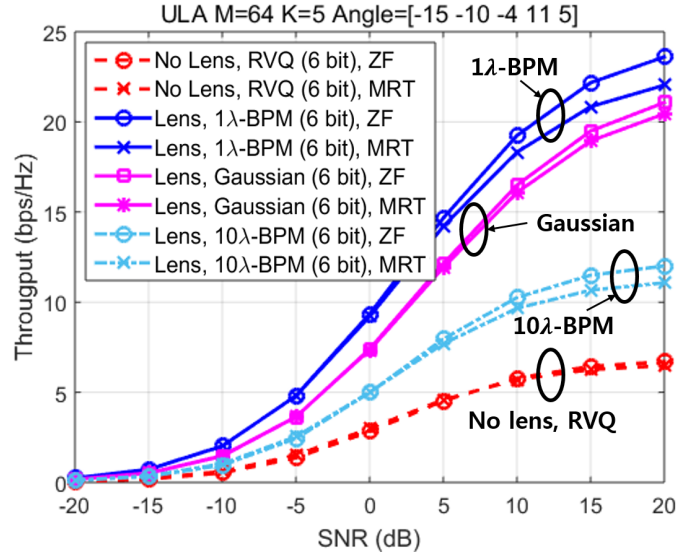


Figure 14: Achievable sum rate of massive MIMO systems with and without the RF lens (Low-complexity estimation for power distribution included).

Indeed, one can simply infer from Fig. 13 that if feedback bits in the MVCQ codebook increases (2 bit \rightarrow 6 bit), rising simultaneously to a certain level is the throughput of the proposed system using the ZF and MRT precoding method. The case where a ZF precoder is used shows more gain in total throughput, which is about 1.96 bps/Hz, while the MRT precoder case showed a slight performance gain, 1.38 bps/Hz at 10 dB SNR.

Figure 14 compares the achievable sum rate performance of several codebook generation methods in MVCQ. We consider the situation where five users having -15° , -10° , -4° , 11° , and 5° in a cell. Low-complexity estimations for power distribution include Gaussian and sub-BPM. For specifying Gaussian distribution, peak power location, y_θ , is given by $y_\theta = (\frac{\theta}{90})(\frac{D}{8})$, and the average power spread, V_θ , as 3. The sampling distance is given as 10λ for sub-BPM. As shown in the figure, there is performance degradation in both codebook generation methods compared to 1λ -BPM. 10λ -BPM is far lower than the 1λ -BPM in the high SNR regime, but still surpass the RVQ case. Although Gaussian estimation comes close to 1λ -BPM and significantly reduces the codebook generation complexity, it may be complicated to decide the parameter y_θ , V_θ may be complicated in practical situation. Two variables may be a function of AoA, θ , lens aperture, D , or even more. This is an issue for future work.

VII. CONCLUSION

In this paper, the RF lens-embedded massive MIMO system was found to significantly reduce the feedback overhead in conventional massive MIMO systems. We adopted beam propagation method (BPM) to calculate the propagation and the focusing of the incident beams controlled by the RF lens. To verify the accuracy of BPM, we fabricated an RF lens operating at mmWave and compared theoretical results with measurement data. BPM was also utilized in the construction

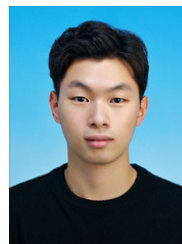
of our new channel model. A new channel quantization-based codebook method, MVCQ, was proposed to generate adaptive codebooks that could reflect multi-channel variances. Analytical and numerical results confirmed that the proposed MVCQ codebook achieved significant performance throughput gain, especially when MRT precoders were used.

ACKNOWLEDGMENT

The authors would like to thank Dr. B.-N. Kim, Mr. M. Jeong, and Mr. C. Kim for their helpful discussions.

REFERENCES

- [1] T. Kwon, Y. G. Lim, and C.-B. Chae, "Limited channel feedback for RF lens antenna based massive MIMO systems," *Proc. IEEE Int. Conf. Computing, Networking and Comm. (ICNC)*, pp. 6–10, Feb. 2015.
- [2] A. Goldsmith, S. A. Jafar, N. Jindal, and S. Vishwanath, "Capacity limits of MIMO channels," *IEEE Jour. Select. Areas in Comm.*, vol. 21, no. 5, pp. 684–702, Jun. 2003.
- [3] D. Gesbert, M. Kountouris, R. W. Heath, Jr., C.-B. Chae, and T. Salzer, "Shifting the MIMO paradigm: From single user to multiuser communications," *IEEE Sig. Proc. Mag.*, vol. 24, no. 5, pp. 36–46, Oct. 2007.
- [4] Q. Spencer, A. L. Swindlehurst, and M. Haardt, "Zero-forcing methods for downlink spatial multiplexing in multiuser MIMO channels," *IEEE Trans. Sig. Proc.*, vol. 52, pp. 462–471, Feb. 2004.
- [5] C.-B. Chae, D. Mazzarese, N. Jindal, and R. W. Heath, Jr., "Coordinated beamforming with limited feedback in the MIMO broadcast channel," *IEEE Jour. Select. Areas in Comm.*, vol. 26, no. 8, pp. 1505–1515, Oct. 2008.
- [6] C.-B. Chae and R. W. Heath, Jr., "On the optimality of linear multiuser MIMO beamforming for a two-user two-input multiple-output broadcast system," *IEEE Sig. Proc. Lett.*, vol. 16, no. 2, pp. 117–120, Feb. 2009.
- [7] J. G. Andrews, S. Buzzi, W. Choi, S. V. Hanly, A. Lozano, A. C. K. Soong, and J. C. Zhang, "What will 5G be?" *IEEE Jour. Select. Areas in Comm.*, vol. 32, no. 6, pp. 1065–1082, Jun. 2014.
- [8] T. L. Marzetta, "Noncooperative cellular wireless with unlimited numbers of base station antennas," *IEEE Trans. Wireless Comm.*, vol. 9, no. 11, pp. 3590–3600, Nov. 2010.
- [9] F. Rusek, D. Persson, B. K. Lau, E. G. Larsson, T. L. Marzetta, O. Edfors, and F. Tufvesson, "Scaling up MIMO: Opportunities and challenges with very large arrays," *IEEE Sig. Proc. Mag.*, vol. 30, no. 1, pp. 40–60, Jan. 2013.
- [10] H. Q. Ngo, E. G. Larsson, and T. L. Marzetta, "Energy and spectral efficiency of very large multiuser MIMO systems," *IEEE Trans. Comm.*, vol. 61, no. 4, pp. 1436–1449, 2011.
- [11] F. Boccardi, R. W. Heath, Jr., A. Lozano, T. L. Marzetta, and P. Popovski, "Five Disruptive technology directions for 5G," *IEEE Comm. Mag.*, vol. 52, no. 2, pp. 74–80, Feb. 2014.
- [12] J. Jang, M. Chung, H. Hwang, Y.-G. Lim, H. Yoon, T. Oh, B. Min, Y. Lee, K. Kim, C.-B. Chae, and D.-K. Kim, "Smart small cell for 5G: From theoretical feasibility to prototype results," *submitted to IEEE Wireless Comm. Mag.*, 2015, also available at arXiv: 1506.09109.
- [13] Y.-G. Lim, C.-B. Chae, and G. Caire, "Performance analysis of massive MIMO for cell-boundary users," *to appear in IEEE Trans. Wireless Comm.*
- [14] D. J. Love, R. W. Heath, Jr., V. K. N. Lau, D. Gesbert, B. D. Rao, and M. Andrews, "An overview of limited feedback in wireless communication systems," *IEEE Jour. Select. Areas in Comm.*, vol. 26, no. 8, pp. 1341–1365, Oct. 2008.
- [15] K. Huang, J. G. Andrews, and R. W. Heath, Jr., "Performance of orthogonal beamforming for SDMA with limited feedback," *IEEE Trans. on Veh. Technol.*, vol. 58, no. 1, pp. 152–164, Jan. 2009.
- [16] N. Jindal, "MIMO broadcast channels with finite-rate feedback," *IEEE Trans. Info. Th.*, vol. 52, no. 11, pp. 5045–5060, Nov. 2006.
- [17] D. J. Love, R. W. Heath, Jr., and T. Strohmer, "Grassmannian beamforming for multiple-input multiple-output wireless systems," *IEEE Trans. Info. Th.*, vol. 49, no. 10, pp. 2735–2747, Oct. 2003.
- [18] T. Inoue and R. W. Heath, Jr., "Geodesic prediction for limited feedback multiuser MIMO systems in temporally correlated channels," *Proc. IEEE Radio Wireless Symp.*, pp. 167–170, Jan. 2009.
- [19] Y. G. Lim and C.-B. Chae, "Compressed channel feedback for correlated massive MIMO systems," *Proc. IEEE Int. Conf. on Comm.*, 2014.
- [20] M. S. Sim, J. Park, C.-B. Chae, and R. W. Heath, Jr., "Compressed Channel Feedback for Correlated Massive MIMO Systems," *to appear in IEEE/KICS Journal of Comm. and Networks*, 2015.
- [21] L. C. Godara, *Handbook of antennas in wireless communications*. CRC Press, 2001.
- [22] Z. P. S. Hollung and A. Cox, "A bi-directional quasi-optical lens amplifier," *IEEE Trans. Microwave Theory Tech.*, vol. 45, no. 12, pp. 2352–2357, Dec. 1997.
- [23] Z. Popovic and A. Mortazawi, "Quasi-optical transmit/receive front ends," *IEEE Trans. Microwave Theory Tech.*, vol. 46, no. 11, pp. 1964–1975, Nov. 1998.
- [24] J. Lau and S. Hum, "A planar reconfigurable aperture with lens and reflectarray modes of operation," *IEEE Trans. Microwave Theory Tech.*, vol. 58, no. 12, Dec. 2010.
- [25] A. Sayeed and N. Behdad, "Continuous aperture phased MIMO: A new architecture for optimum line-of-sight links," *in Proc. IEEE APSURSI*, pp. 293–296, Jul. 2011.
- [26] J. Brady, N. Behdad, and A. M. Sayeed, "Beamspace MIMO for millimeter-wave communications: system architecture, modeling, analysis, and measurements," *IEEE Trans. Antennas Propag.*, vol. 61, no. 7, pp. 3814–3827, Jul. 2013.
- [27] Y. Zeng, R. Zhang, and Z. N. Chen, "Electromagnetic lens focusing antenna enabled massive MIMO: performance improvement and cost reduction," *IEEE Jour. Select. Areas in Comm.*, Sep. 2014.
- [28] J. V. Roey, J. van der Donk, and P. E. Lagasse, "Beam-propagation method: analysis and assessment," *J. Opt. Soc. Am.*, vol. 71, no. 7, pp. 803–810, 1981.
- [29] G. A. Ediss, S.-J. P. Wang, and N. J. Keen, "Quasi-optical components for 230GHz and 460GHz," *Inst. Elec. Eng.*, pp. 99–106, 1985.
- [30] B. Scannell, C. Nightingale, G. O'Connors, and A. Philpott, "Gaussian beamwaist and radiation pattern measurements of a quasi-optical radiometer," *Proc. 6th Int. Conf. Antenna Propag., ICAP-89, Coventry*, pp. 383–389, 1989.
- [31] R. B. Ertel, P. Carderi, K. W. Sowerby, T. S. Rappaport, and J. H. Reed, "Overview of spatial channel models for antenna array communication systems," *Proc. IEEE Conf. Pers. Wireless Commun.*, pp. 10–22, Feb. 1998.
- [32] A. Forenza, D. J. Love, and R. W. Heath, Jr., "Simplified spatial correlation models for clustered MIMO channels with different array configurations," *IEEE Trans. on Veh. Technol.*, vol. 56, no. 4, pp. 1924–1934, Jul. 2007.
- [33] 3GPP TR 25.996 V12.0.0, "Spatial channel model for Multiple Input Multiple Output (MIMO) simulations (Release 12)," Sep. 2014.
- [34] Y. Zeng and R. Zhang, "Millimeter Wave MIMO with Lens Antenna Array: A New Path Division Multiplexing Paradigm," *submitted for possible journal publication*, 2015, available at arXiv: 1507.01699.
- [35] J. W. Goodman, *Introduction to fourier optics*. McGraw-Hill, 1996.
- [36] R. C. Hansen, "Focal region characteristics of focused array antennas," *IEEE Trans. Antennas Propag.*, vol. AP-33, pp. 586–593, Dec. 1985.
- [37] K. Chang, Ed., *Handbook of Microwave and Optical Components*. Wiley, vol. 1.
- [38] M. N. Afsar and K. J. Button, "Millimeter-wave dielectric measurements of materials," *Proc. IEEE*, vol. 73, no. 1, pp. 131–153, 1985.



Tae-hoon Kwon (S'13) received his B.S. degree in the School of Integrated Technology from Yonsei University, Korea, in 2014. He is now with the School of Integrated Technology, at the same university and is working toward the Ph.D. degree. His research interest includes emerging communication technologies.



Yeon-Geun Lim (S'12) received his B.S. degree in Information and Communications Engineering from Sungkyunkwan University, Korea in 2011. He is now with the School of Integrated Technology, Yonsei University, Korea and is working toward the Ph.D. degree. His research interest includes massive MIMO and interference management techniques for smart small cell networks.



Byung-Wook Min ('S03-'M08) was born in Seoul, Korea. He received the B.S. degree from Seoul National University, Seoul, Korea, in 2002, and the M.S. and Ph.D. degrees in electrical engineering and computer science from The University of Michigan at Ann Arbor, in 2004 and 2007, respectively. In 2006 and 2007, he was a Visiting Scholar with the University of California at San Diego, La Jolla. From 2008 to 2010, he was a Senior Engineer with Qualcomm Inc. In 2011, he joined the School of Electrical and Electronic Engineering, Yonsei

University, Seoul, Korea, as an Assistant Professor. His research interests include Si/SiGe RF integrated circuits (RFICs), microwave packaging, and RF microelectromechanical systems (MEMS) for microwave and millimeter-wave applications. He was a recipient of the Samsung Scholarship (2002–2007).



Chan-Byoung Chae ('S06-'M09-'SM12) is Associate Professor in the School of Integrated Technology, College of Engineering, Yonsei University, Korea. He was a Member of Technical Staff (Research Scientist) at Bell Laboratories, Alcatel-Lucent, Murray Hill, NJ, USA from June 2009 to Feb 2011. Before joining Bell Laboratories, he was with the School of Engineering and Applied Sciences at Harvard University, Cambridge, MA, USA as a Post-Doctoral Research Fellow. He received the Ph.D. degree in Electrical and Computer Engineering from

The University of Texas (UT), Austin, TX, USA in 2008, where he was a member of the Wireless Networking and Communications Group (WNCG). Prior to joining UT, he was a Research Engineer at the Advanced Research Lab., the Telecommunications R&D Center, Samsung Electronics, Suwon, Korea, from 2001 to 2005. He was a Visiting Scholar at the WING Lab, Aalborg University, Denmark in 2004 and at University of Minnesota, MN, USA in August 2007. While having worked at Samsung, he participated in the IEEE 802.16e standardization, where he made several contributions and filed a number of related patents from 2004 to 2005. His current research interests include capacity analysis and interference management in energy-efficient wireless mobile networks and nano (molecular) communications.

He has served/serves as an Editor for the IEEE Trans. on Wireless Communications, IEEE Trans. Molecular, Biological, and Multi-scale Comm., IEEE Trans. on Smart Grid, IEEE ComSoc Technology News, and IEEE/KICS Jour. of Comm. Networks. He was a Guest Editor for the IEEE Jour. Sel. Areas in Comm. (special issue on molecular, biological, and multi-scale comm.). He is an IEEE Senior Member.

Dr. Chae was the recipient/co-recipient of the IEEE INFOCOM Best Demo Award (2015), the IEIE/IEEE Joint Award for Young IT Engineer of the Year (2014), the KICS Haedong Young Scholar Award (2013), the IEEE Signal Processing Magazine Best Paper Award (2013), the IEEE ComSoc AP Outstanding Young Researcher Award (2012), the IEEE Dan. E. Noble Fellowship Award (2008), two Gold Prizes (1st) in the 14th/19th Humantech Paper Contest, and the KSEA-KUSCO scholarship (2007). He also received the Korea Government Fellowship (KOSEF) during his Ph.D. studies.